

**1 Conceptual model analysis of the influence of**  
**2 temperature feedbacks on polar amplification**

Ashley E. Payne,<sup>1</sup> Malte F. Jansen,<sup>2</sup> Timothy W. Cronin,<sup>3</sup>

---

<sup>1</sup>Department of Earth System Science,  
University of California, Irvine, California,  
USA.

<sup>2</sup>Department of the Geophysical Sciences,  
The University of Chicago, Chicago, Illinois,  
USA.

<sup>3</sup>Department of Earth and Planetary  
Sciences, Harvard University, Cambridge,  
Massachusetts, USA.

3 The role of temperature feedbacks in polar amplification of climate change  
4 is examined by comparing the response of idealized high- and low-latitude  
5 atmospheric columns to greenhouse-gas forcing. An analytic expression for  
6 the surface polar amplification factor is derived with a one-layer atmospheric  
7 model, and compared to a more detailed column model with two radiative  
8 transfer schemes. The modeled temperature profiles result from competition  
9 between the stabilizing influences of atmospheric heat flux convergence and  
10 atmospheric solar heating (dominant at high latitudes), and the destabiliz-  
11 ing influence of surface solar heating (dominant at low latitudes). For a sta-  
12 ble high-latitude radiative-advective atmosphere, the lapse rate increases with  
13 greenhouse-gas forcing, leading to a positive feedback, and is dependent on  
14 the nature of the forcing – pointing to limitations of the traditional forcing-  
15 feedback framework. For a low-latitude radiative-convective atmosphere, the  
16 lapse rate decreases, leading to a negative feedback.

## 1. Introduction

17 Surface temperatures in the Arctic have increased at twice the rate of the global av-  
18 erage [Meehl *et al.*, 2007]. The strengthened response of surface warming at high lati-  
19 tudes is referred to as polar amplification. The surface albedo feedback, or absorption of  
20 more shortwave radiation with warming due to ice loss, is thought to play a large role  
21 in present-day polar amplification [Manabe and Wetherald, 1975; Screen and Simmonds,  
22 2010]. However, this positive feedback cannot fully explain polar amplification in idealized  
23 model simulations and in paleoclimate records of both natural and forced climate variabil-  
24 ity where albedo feedbacks are reduced or absent [Held, 1978; Manabe and Stouffer, 1980;  
25 Hall, 2004; Winton, 2006; Miller *et al.*, 2010; Roe *et al.*, 2015]. The additional feedbacks  
26 that contribute to polar amplification can be difficult to analyze because they interact not  
27 only with the surface albedo feedback, but also with changes in atmospheric [Graversen  
28 *et al.*, 2008; Yang *et al.*, 2010] and oceanic [Chylek *et al.*, 2009] energy transport.

29 A large fraction of polar amplification can be attributed to longwave radiative feed-  
30 backs [Winton, 2006], which include the effects of clouds [Vavrus, 2004], water vapor [Gra-  
31 versen and Wang, 2009] and temperature [Pithan and Mauritsen, 2014]. Longwave tem-  
32 perature feedbacks can be further broken down into the Planck feedback, or change in  
33 outgoing radiation due to vertically uniform warming, and the lapse-rate feedback, or  
34 change in outgoing radiation due to deviations from vertically uniform warming. Recent  
35 work has highlighted the lapse-rate feedback as a possible driver of polar amplification due  
36 to its differing response between high and lower latitudes [Lu and Cai, 2010; Bintanja  
37 *et al.*, 2011; Pithan and Mauritsen, 2014; Graversen *et al.*, 2014]. However, it is diffi-

38 cult to consider the lapse-rate feedback independently within a global model [*Graversen*  
39 *et al.*, 2014], and the basic controls on the high-latitude lapse rate and its sensitivity to  
40 climate remain poorly understood. A simplified method is needed to better understand  
41 high-latitude lapse rate changes and their role in polar amplification.

42 We use a hierarchy of conceptual models to isolate the lapse-rate feedback and inves-  
43 tigate how it contributes to polar amplification. We analyze the response of two climate  
44 regimes: (1) convectively stable, high-latitude (HL) radiative-advective equilibrium (small  
45 surface solar absorption, large net atmospheric heating), and (2) convectively neutral,  
46 low-latitude (LL) radiative-convective equilibrium (large surface solar absorption, small  
47 net atmospheric heating). We examine the sensitivity of surface temperature to varying  
48 surface solar absorption, atmospheric heating, and total longwave optical depth of the  
49 atmosphere. For both a simple single-layer atmosphere and a more detailed dry column  
50 model of the atmosphere, we find that the lapse-rate feedback amplifies the high-latitude  
51 surface temperature response to changing greenhouse gas concentrations. We conclude  
52 with a brief investigation of how inclusion of the water vapor feedback modifies our results.

## 53 2. Methods

54 We use two models: (1) a simple two-level, one-dimensional energy balance model  
55 (EBM) and (2) a 26-layer column model, based on the Climate Modelling and Diagnostics  
56 Toolkit (CliMT) [*Caballero et al.*, 2013]. In the EBM, the lower level represents the  
57 surface ( $p_S = 1000$  hPa,  $T_S$ ) and the upper level represents the mid-troposphere ( $p_A =$   
58  $500$  hPa,  $T_A$ ), referred to as the “atmosphere” (Figure 1 shows a schematic of model

59 inputs). Equilibrium implies energy balance at both levels:

$$0 = F_S - F_C + \epsilon\sigma T_A^4 - \sigma T_S^4, \quad (\text{surface}) \quad (1)$$

$$0 = F_A + F_C + \epsilon\sigma T_S^4 - 2\epsilon\sigma T_A^4, \quad (\text{atmosphere}) \quad (2)$$

60 where  $\epsilon$  is the atmospheric emissivity,  $\sigma$  is the Stefan-Boltzmann constant, and  $T_S$  and  
 61  $T_A$  are the surface and atmospheric temperatures, respectively. Eqs. 1 and 2 include  $F_C$   
 62 to account for vertical convective heat transport. Convection is triggered when  $(T_S -$   
 63  $T_A)$  exceeds a temperature-dependent convective lapse rate,  $\Delta_T$ , defined as the vertical  
 64 temperature difference in units of K.  $\Delta_T$  is computed in the EBM by following a moist  
 65 adiabat from  $p_S$  to  $p_A$ . For current low-latitude surface temperatures,  $\Delta_T \approx 31$  K, and  
 66  $\Delta_T$  decreases with warming by  $\gamma \equiv d\Delta_T/dT_s \approx -0.6$  K/K. A current high-latitude  $T_S =$   
 67 260 K gives a  $\Delta_T^{HL} \approx 44$  K – larger than any of our high-latitude EBM solutions.

68 We use  $\Delta_T$  and the top-of-atmosphere energy balance to solve for the low-latitude  
 69 surface and atmospheric temperatures in the EBM:

$$F_S + F_A = (1 - \epsilon)\sigma T_S^4 + \epsilon\sigma(T_S - \Delta_T)^4, \quad (3)$$

$$T_A = T_S - \Delta_T. \quad (4)$$

70 We use  $F_C = 0$  to solve for the high-latitude  $T_S$  and  $T_A$ :

$$\sigma T_S^4 = \frac{2F_S + F_A}{(2 - \epsilon)}, \quad (5)$$

$$\sigma T_A^4 = \frac{\epsilon F_S + F_A}{\epsilon(2 - \epsilon)}, \quad (6)$$

71 which is physical so long as the column is convectively stable, that is  $T_S - T_A < \Delta_T$  [see  
 72 also *Abbot and Tziperman, 2009*].

73 The energy sources are  $F_S$ , which represents the surface shortwave absorption (LL:  
74  $215.1 \text{ W m}^{-2}$ , HL:  $34.9 \text{ W m}^{-2}$ ), and  $F_A$ , which represents the sum of atmospheric heat  
75 flux convergence (LL:  $-64.2 \text{ W m}^{-2}$ , HL:  $100.8 \text{ W m}^{-2}$ ) and direct atmospheric shortwave  
76 absorption (LL:  $90.9 \text{ W m}^{-2}$ , HL:  $40.2 \text{ W m}^{-2}$ ). Values for these energy sources for repre-  
77 sentative low-latitude (zonal-mean from  $10^\circ - 15^\circ\text{N}$ ) and high-latitude (zonal-mean from  
78  $80^\circ - 85^\circ\text{N}$ ) regions are derived from climatological (1979 - 2015) averages from MERRA  
79 reanalysis [Rienecker et al., 2011]. In general,  $F_S$  should also account for both ocean heat  
80 flux convergence and subsurface heat storage. We neglect ocean heat flux convergence  
81 because it is small in both regions [Trenberth and Caron, 2001; Serreze et al., 2008]. We  
82 also neglect subsurface heat storage because we focus on annual-mean conditions; apply-  
83 ing the model to understand seasonal warming patterns would require including surface  
84 heat storage in  $F_S$ .

85 The column model equivalent of the EBM uses a grey-gas radiative scheme coupled to  
86 a slab ocean and simple turbulence and convection schemes. Turbulence is parameterized  
87 using a bulk formula for surface sensible heat exchange and weak vertical diffusion of  
88 potential temperature (diffusivity,  $\kappa = 0.02 \text{ m}^2\text{s}^{-1}$ ). Convection is parameterized by hard  
89 adjustment to the moist adiabatic lapse rate. The influence of greenhouse gases on surface  
90 and atmospheric temperatures is represented in the EBM by the atmospheric emissivity,  
91  $\epsilon$  ( $0 < \epsilon \leq 1$ ), and in the grey-gas column model by the optical depth,  $\tau = \tau_0(1 - p/p_S)^2$   
92 (where  $\tau_0$  is the total column optical depth). A water vapor feedback is not incorporated  
93 into either model.

94 In a second configuration of the column model, we use a multi-band radiative scheme  
 95 based on the Column Radiation Model by NCAR’s Community Climate Model (CCM3).  
 96 In this configuration, the ozone profile is taken from MERRA reanalysis, the model is  
 97 forced by annually-averaged insolation (LL:  $411.9 \text{ W m}^{-2}$ , HL:  $179.0 \text{ W m}^{-2}$ ), and  $F_A$  is  
 98 limited to the contribution from meridional heat flux convergence (the radiative scheme  
 99 calculates shortwave atmospheric absorption). The surface albedo is adjusted (LL: 0.11,  
 100 HL: 0.53) so that temperature profiles approximate reanalysis (averaged from 2010 to  
 101 2015) with  $p\text{CO}_2 = 400 \text{ ppmv}$ . We run this model with both fixed specific humidity  
 102 (fixed-q) and fixed relative humidity (fixed-RH) to examine the role of temperature and  
 103 water vapor feedbacks.

104 In both the grey-gas and CCM3 models, atmospheric heat flux convergence is parame-  
 105 terized following a square-root distribution:

$$Q(p) = \frac{3F_A}{2(p_S - p_T)} \left[ \frac{(p - p_T)}{(p_S - p_T)} \right]^{1/2} \quad (7)$$

106 going to zero at the tropopause ( $p_T^{LL} = 90 \text{ hPa}$  and  $p_T^{HL} = 275 \text{ hPa}$ ) [roughly approximating  
 107 the tropospheric heat transport profile shown in *Oort, 1974*].

### 3. Theory

108 We start with an analytic investigation of the EBM’s sensitivity of surface temperatures  
 109 to (1) small changes in atmospheric emissivity ( $\delta T_S/\delta\epsilon$ ), and to (2) fixed-flux forcing  
 110 ( $\delta T_S/\delta F$ ), where  $F$  represents either radiative forcing or advective heat flux convergence.  
 111 We focus on the two representative climate regimes described above to explore differences  
 112 between high and low latitudes.

### 3.1. Sensitivity to emissivity

113 To analyze the response of surface temperatures to a small change in the atmospheric  
 114 emissivity, we substitute  $\epsilon + \delta\epsilon$  and  $T_S + \delta T_S$  for  $\epsilon$  and  $T_S$ , respectively, into the EBM  
 115 (Eqs. 3 and 5). Note that in the real climate system, both local feedbacks and changes in  
 116 heat transport would also alter  $F_S$  and  $F_A$ ; our simplifying assumption of constant  $F_S$  and  
 117  $F_A$  is intended to isolate the role of temperature feedbacks. For infinitesimal  $\delta T_S$  and  $\delta\epsilon$ ,  
 118 this yields for low-latitude ( $\delta T_S^{LL}$ ) and high-latitude ( $\delta T_S^{HL}$ ) surface temperature change:

$$\delta T_S^{LL} = \frac{T_S^4 - (T_S - \Delta_T)^4}{4(1 - \epsilon)T_S^3 + 4\epsilon(1 - \gamma)(T_S - \Delta_T)^3} \delta\epsilon, \quad (8)$$

$$\delta T_S^{HL} = \frac{T_S}{4(2 - \epsilon)} \delta\epsilon. \quad (9)$$

119 Assuming that the low-latitude lapse rate,  $\Delta_T$ , is much smaller than  $T_S$ , we can simplify  
 120 Eq. 8 to:

$$\delta T_S^{LL} \approx \frac{\Delta_T}{1 - \epsilon\gamma} \delta\epsilon. \quad (10)$$

121 Equation 9 shows that  $\delta T_S^{HL}$  is proportional to the high-latitude surface temperature  
 122 and increases with emissivity. Equation 10 shows that  $\delta T_S^{LL}$  depends on  $\Delta_T$  and its  
 123 sensitivity to temperature,  $\gamma$ . Assuming equal changes in emissivity, we can estimate a  
 124 polar amplification factor using Eqs. 9 and 10:

$$\frac{\delta T_S^{HL}}{\delta T_S^{LL}} \approx \frac{(1 - \epsilon\gamma)T_S^{HL}}{4(2 - \epsilon)\Delta_T}. \quad (11)$$

125 For  $\Delta_T \approx 33$  K,  $\gamma \approx -0.6$ , and  $\epsilon = 0.9$ , we find a polar amplification factor of roughly 2.6.  
 126 Note that this factor is an approximation because higher-order terms in Eq. 8 are omitted  
 127 in Eq. 10; exact calculation by dividing Eq. 9 by Eq. 8 gives a polar amplification factor

128 of 2.2. Note also that Eq. 11 could be multiplied by  $\delta\epsilon^{HL}/\delta\epsilon^{LL}$  to account for unequal  
 129 changes in emissivity due to meridional variation in the water vapor feedback.

130 The polar amplification in the EBM results from the differing lapse rate response, and  
 131 cannot be attributed simply to the differing Planck feedback. In the scenario of a fixed  
 132 lapse rate (Eq. 10 with  $\gamma = 0$ ), the temperature response depends to first order only on  
 133 the lapse rate itself and is independent of  $T_S$ . Therefore, at the same fixed lapse rate,  
 134 colder high-latitude surface temperatures alone would not lead to polar amplification in  
 135 response to atmospheric emissivity changes. Considering this scenario from a forcing-  
 136 feedback perspective, a weaker Planck feedback at cold high latitudes would be offset by  
 137 a similarly weaker radiative forcing.

### 3.2. Sensitivity to forcing

138 The sensitivity to a unit forcing of  $1 \text{ W m}^{-2}$  allows us to calculate Planck and lapse-  
 139 rate feedback parameters for the atmosphere in each region, and to determine whether  
 140 the feedbacks depend on the type of forcing. We investigate the sensitivity of surface  
 141 temperature to three types of forcing: surface-based ( $\delta T_S/\delta F_S$ ), atmospheric ( $\delta T_S/\delta F_A$ )  
 142 and emissivity-induced radiative forcing ( $\delta T_S/\delta F_R$ ). Here  $\delta F_R$  is the change in top-of-  
 143 atmosphere energy balance due to a small change in atmospheric emissivity, holding  $T_S$   
 144 and  $T_A$  fixed:

$$\delta F_R \equiv (\sigma T_S^4 - \sigma T_A^4)\delta\epsilon. \quad (12)$$

145 The radiative forcing from an increase in atmospheric emissivity (due to greenhouse gases)  
 146 depends on the difference between surface and atmospheric temperature – larger at low  
 147 latitudes than high latitudes. The radiative forcing for our two representative columns is

148 given by:

$$\delta F_R^{LL} = \left[ \sigma T_S^4 - \sigma (T_S - \Delta_T)^4 \right] \delta \epsilon, \quad (13)$$

$$\delta F_R^{HL} = \left[ \frac{\sigma T_S^4}{2} - \frac{F_A}{2 - \epsilon} \left( \frac{1}{\epsilon} - \frac{1}{2} \right) \right] \delta \epsilon. \quad (14)$$

149 We focus first on the sensitivity of  $T_S$  to forcing in low-latitude radiative-convective equi-  
 150 librium. We perturb Eq. 3 to determine sensitivity of  $T_S$  to surface and atmospheric  
 151 forcing, and divide Eq. 8 by Eq. 13 to determine the sensitivity of  $T_S$  to emissivity-  
 152 induced radiative forcing; all three sensitivities turn out to be equal:

$$\frac{\delta T_S^{LL}}{\delta F_S} = \frac{\delta T_S^{LL}}{\delta F_A} = \frac{\delta T_S^{LL}}{\delta F_R} = \frac{1}{4\sigma T_S^3(1 - \epsilon) + 4\epsilon\sigma(1 - \gamma)(T_S - \Delta_T)^3}. \quad (15)$$

153 The negative inverse of Eq. 15 gives the total feedback of the column, which, in this simpli-  
 154 fied model framework, is only a temperature feedback:  $\lambda_T = -\delta F / \delta T_S$ . This temperature  
 155 feedback in turn can be broken into Planck and lapse rate components:

$$\begin{aligned} \lambda_P^{LL} &= -4\sigma \left[ (1 - \epsilon)T_S^3 + \epsilon(T_S - \Delta_T)^3 \right] \\ \lambda_{LR}^{LL} &= 4\sigma\epsilon\gamma(T_S - \Delta_T)^3, \end{aligned} \quad (16)$$

156 where the Planck feedback ( $\lambda_P$ ) is the response to a vertically uniform warming and the  
 157 lapse-rate feedback is the residual of  $\lambda_T - \lambda_P$ . Low-latitude feedbacks are independent of  
 158 the type of forcing, and because the moist convective lapse rate decreases with temperature  
 159 ( $\gamma < 0$ ), the low-latitude lapse-rate feedback is negative.

160 For high-latitude radiative-advective equilibrium, we perform a similar analysis: we  
 161 perturb Eq. 5 to determine the sensitivity of  $T_S$  to  $F_S$  or  $F_A$ , and divide Eq. 9 by Eq. 14  
 162 to determine the sensitivity of  $T_S$  to  $F_R$ :

$$\frac{\delta T_S^{HL}}{\delta F_S} = \frac{1}{4\sigma T_S^3(1 - \frac{\epsilon}{2})}, \quad (17)$$

$$\frac{\delta T_S^{HL}}{\delta F_A} = \frac{1}{8\sigma T_S^3(1 - \frac{\epsilon}{2})}, \quad (18)$$

$$\frac{\delta T_S^{HL}}{\delta F_R} = \frac{1}{4\sigma T_S^3(1 - \frac{\epsilon}{2}) - \frac{4F_A}{T_S}(\frac{1}{\epsilon} - \frac{1}{2})}. \quad (19)$$

163 These sensitivities all differ from each other. The sensitivity of surface temperature to  
 164 surface forcing is exactly double that to atmospheric forcing [previously noted by *Abbot*  
 165 *and Tziperman*, 2008], and the sensitivity of surface temperature to emissivity-induced  
 166 radiative forcing is larger still (the second term in the denominator of Eq. 19 reveals  
 167 that  $\delta T_S^{HL}/\delta F_R$  is always increased relative to  $\delta T_S^{HL}/\delta F_S$  because  $F_A > 0$ ). Note that  
 168 the emissivity-induced radiative forcing will be negative if the surface is colder than the  
 169 atmosphere ( $T_S < T_A$ ), but the surface temperature nonetheless increases with increasing  
 170 emissivity.

171 The Planck feedback is given by the same expression  $\lambda_P = -4\sigma [(1 - \epsilon)T_S^3 + \epsilon T_A^3]$  re-  
 172 gardless of forcing. Therefore, one can interpret the differing sensitivity to forcing of  
 173 the high-latitude equilibrium as arising from differences in the lapse-rate response. The  
 174 fixed Planck feedback, along with the total temperature feedback from Eqs. 17 - 19  
 175 ( $\lambda_T = -\delta F/\delta T_S$ ), allows us to calculate the forcing-specific lapse-rate feedbacks:

$$\lambda_{LR}^{HL}(F_S) = 4\sigma\epsilon \left( T_A^3 - \frac{T_S^3}{2} \right), \quad (20)$$

$$\lambda_{LR}^{HL}(F_A) = -4\sigma \left( T_S^3 - \epsilon T_A^3 \right), \quad (21)$$

$$\lambda_{LR}^{HL}(F_R) = 4\sigma\epsilon \left( T_A^3 - \frac{T_S^3}{2} \right) + \frac{4F_A}{T_S} \left( \frac{1}{\epsilon} - \frac{1}{2} \right). \quad (22)$$

176 The sign of the lapse-rate feedback differs across forcings. It can be shown from Eqs. 20 -  
 177 22 that the lapse-rate feedback is always positive for surface forcing or radiative forcing,  
 178 and always either negative or zero for atmospheric heat flux forcing. The differences

179 among Eqs. 17 - 19 and 20 - 22 point to limitations of the conventional forcing-feedback  
180 analysis framework for understanding climate change at high latitudes. Changes in the  
181 lapse rate depend on the nature of the forcing, rather than depending solely on the surface  
182 temperature.

#### 4. Model results

183 Next, we compare predictions in section 3 to solutions of both the EBM and the grey-  
184 gas column model over a range of emissivities and optical depths. In Figs. 2a and 2b,  
185 we show high-latitude (blue) and low-latitude (orange) surface and atmospheric tempera-  
186 tures. Both models show polar amplification consistent with the analytical approximation  
187 in Eq. 11. The high-latitude surface temperature response is amplified by a factor of 2.2  
188 in the EBM (near  $\epsilon = 0.9$ ) and by 2.2 in the grey-gas model (near  $\tau_0 = 2.7$ , chosen so  
189 that the low-latitude lapse rate is similar to the EBM). The increased sensitivity of high-  
190 latitude surface temperatures is attributable to the net atmospheric heat import, which  
191 stabilizes the atmosphere to convection and allows radiative forcing to drive the lapse rate  
192 toward a convectively neutral state. Both models agree on the magnitude of the lapse  
193 rate increase at high latitudes and decrease at low latitudes (dashed versus solid lines in  
194 Fig. 2c). Changes in lapse rate with increasing optical depth lead to a positive feedback  
195 at high latitudes, but a negative feedback at low latitudes. At low optical depth, the  
196 high-latitude lapse rate response in both models is so strong that the atmospheric tem-  
197 perature decreases with increasing optical depth. This limit resembles the stratosphere  
198 (also optically thin in the longwave and heated in the shortwave), which also cools in  
199 response to increasing greenhouse gas concentrations [*Hansen et al.*, 1997].

200 We now focus on the sensitivity of the grey-gas column to a fixed change in optical  
201 depth,  $\delta\tau_0 = +0.2$ . We select reference-state  $\tau_0$  to roughly match present-day high- and  
202 low-latitude temperature profiles (compare orange and blue lines to grey lines in Fig. 3a),  
203 parameterizing differences in total optical depth attributable to differences in column  
204 water vapor. We use a reference value of  $\tau_0 = 2.7$  at high latitudes and  $\tau_0 = 4.7$  at  
205 low latitudes. These optical depths give  $T_S^{LL} = 294.8$  K and  $T_S^{HL} = 259.6$  K, with a  
206 slight surface inversion and stable troposphere at high latitudes, and a moist adiabatic  
207 troposphere at low latitudes.

208 Figure 3b provides a detailed picture of the lapse rate changes outlined in Fig. 2. The  
209 temperature sensitivity to a change in optical depth varies vertically and differs between  
210 the two regions. High-latitude warming is concentrated in the lower troposphere and at the  
211 surface, but low-latitude warming is concentrated in the upper troposphere. Although sur-  
212 face warming is polar-amplified, upper-tropospheric warming is tropically-amplified. This  
213 temperature response pattern implies that the meridional temperature gradient weakens  
214 at the surface, but strengthens in the upper-troposphere. The meridional variation in the  
215 vertical structure of warming is a robust feature found in previous research [*Meehl et al.*,  
216 2007; *Lu and Cai*, 2010], and implies changes in poleward atmospheric heat transport [e.g.  
217 *Held*, 1978].

218 Polar amplification inferred from Fig. 3b ( $\delta T_S^{LL} = 0.6$  K,  $\delta T_S^{HL} = 2.8$  K) is much larger  
219 than the factor of about 2 - 3 estimated above. This apparent discrepancy is primarily  
220 a result of the regionally differing optical depths assumed in Fig. 3 (estimates above  
221 assumed similar optical depth in both regions). The radiative forcing in a thick grey

222 atmosphere is approximately proportional to two factors: the relative change of optical  
223 depth ( $\delta\tau_0/\tau_0$ ), and the base-state lapse rate. These two factors approximately compensate  
224 between regions in Fig. 3 –  $\delta\tau_0/\tau_0$  is larger for high latitudes, but the lapse rate is larger  
225 for low latitudes. This compensation makes radiative forcing in the two regions quite  
226 similar ( $\delta F_R^{LL} = 3.3 \text{ W m}^{-2}$ ,  $\delta F_R^{HL} = 3.2 \text{ W m}^{-2}$ ). Therefore, the warming structure  
227 per unit radiative forcing closely resembles the total warming (compare Figs. 3c to 3b).  
228 To investigate the components of the total temperature feedback, we again calculate the  
229 Planck and the lapse-rate feedbacks as in section 3.2. The lapse-rate feedback is strongly  
230 positive at high latitudes ( $\lambda_{LR}^{HL} = 1.8 \text{ W m}^{-2} \text{ K}^{-1}$ ) and negative at low latitudes ( $\lambda_{LR}^{LL} =$   
231  $- 1.8 \text{ W m}^{-2} \text{ K}^{-1}$ ).

232 To investigate the robustness of our findings, we use the CCM3 model to explore the  
233 temperature response to increasing  $\text{CO}_2$ . We compute the sensitivity to  $\text{CO}_2$  doubling for  
234 both fixed specific humidity (without water vapor feedback) and fixed relative humidity  
235 (with water vapor feedback). For both cases, the reference simulation uses  $p\text{CO}_2 = 280$   
236 ppmv with relative humidity set to 60% in the troposphere, and specific humidity in the  
237 stratosphere set to either the value at the tropopause or 60% relative humidity (whichever  
238 is smaller).

239 Figure 4a shows high- and low-latitude temperature profiles for  $p\text{CO}_2 = 280$  ppmv and  
240 560 ppmv compared against reanalysis (compare blue and orange lines to grey lines).  
241 Model profiles are approximately consistent with reanalysis, with notable differences in  
242 the strength of the high-latitude lower-tropospheric inversion – an issue we will return  
243 to below. As in previous models, the lapse rate increases at high latitudes and decreases

244 at low latitudes for a doubling of CO<sub>2</sub> (Figure 4b). Focusing first on the fixed specific  
245 humidity case, we find that surface warming is still polar-amplified, but by a factor of  
246 only 1.6 ( $\delta T_S^{LL} = 0.8$  K,  $\delta T_S^{HL} = 1.3$  K), considerably smaller than in the grey-gas model  
247 (Fig. 3). Part of the decrease in the polar amplification factor owes to a smaller CO<sub>2</sub>  
248 forcing at high latitudes compared to low latitudes (stratosphere-adjusted [*Hansen et al.*,  
249 1997];  $\delta F_R^{LL} = 4.3$  W m<sup>-2</sup>,  $\delta F_R^{HL} = 3.1$  W m<sup>-2</sup>), because optical depth in the CO<sub>2</sub>  
250 band is increased by the same relative amount in the two regions, but the high-latitude  
251 lapse rate is smaller. However, reduced forcing does not fully explain the difference.  
252 Comparison of Fig. 4c to 3c reveals that the low-latitude sensitivity to radiative forcing  
253 is similar between models. However, high-latitude sensitivity depends on the radiation  
254 scheme; the grey-gas model has greatest sensitivity at the surface whereas the CCM3  
255 model has greatest sensitivity at 850 hPa. We speculate that this difference is related to  
256 the atmospheric window (present only in the CCM3 model) – which allows the surface to  
257 radiate directly to space. The presence of a window in the CCM3 model may also lead  
258 to the strong high-latitude inversion. Note that we use only clear-sky radiative transfer;  
259 including the effects of clouds – which act as grey bodies in the longwave – would likely  
260 modify our results.

261 To investigate the effect of the water vapor feedback, we compare results for fixed  
262 specific humidity to a case with fixed relative humidity (compare solid lines to dashed  
263 lines in Fig. 4). Fixing the relative humidity leads to a strong low-latitude water vapor  
264 feedback, canceling the polar amplification seen in previous models ( $\delta T_S^{LL} = 2.4$  K,  $\delta T_S^{HL}$   
265  $= 1.6$  K; Fig. 4b). The water vapor feedback leads to an additional surface warming of 1.6

266 K for low latitudes, but only 0.3 K for high latitudes. The sensitivity of the low-latitude  
267 temperature profile to CO<sub>2</sub> doubling is greatly increased by the water vapor feedback  
268 (Fig. 4b,c), and the warming near the tropopause exceeds 6 K. In contrast, there is  
269 almost no upper-tropospheric warming in the high-latitude profile.

270 The low-latitude water vapor feedback<sup>1</sup> amounts to  $\sim 3.6 \text{ W m}^{-2} \text{ K}^{-1}$ , roughly consistent  
271 with the tropical clear-sky water vapor feedback in global models [*Soden et al.*, 2008].  
272 However, the all-sky water vapor feedback is generally reduced by 25 - 50% due to cloud-  
273 masking effects (missing in our model). Nevertheless, ignoring additional feedbacks or  
274 changes in the heat transport, the water vapor feedback would likely cancel most of the  
275 differential effect of the lapse-rate feedback, leaving little or no polar amplification.

276 The robust signal of polar amplification in moist models and paleoclimate records, even  
277 in the absence of a surface albedo feedback (which amplifies high-latitude warming), thus  
278 indicates the importance of additional processes. One likely candidate is the sensitivity of  
279 meridional heat transport to warming. *Hwang and Frierson* [2010] argue that meridional  
280 energy transport may to first order be approximated by diffusion of moist static energy.  
281 For a given equator-to-pole temperature gradient and relative humidity, the moist static  
282 energy gradient increases with warming due to the curvature of the Clausius-Clapeyron  
283 relation, thus potentially leading to an increase in the meridional energy transport. More-  
284 over, the temperature change patterns in response to doubling CO<sub>2</sub> (Fig. 4b) indicate  
285 an enhanced temperature gradient in the atmosphere, as well as a decrease in the high-  
286 latitude static stability; both responses may favor further enhanced eddy heat transport  
287 [e.g. *Held*, 1978; *Jansen and Ferrari*, 2013]. Investigating the interaction between high-

288 and low-latitude temperature and lapse rate changes and changes in atmospheric heat  
289 transport is an important topic for further work, but beyond the scope of this article.

## 5. Conclusions

290 We analyze the sensitivity of high- and low-latitude surface temperatures to changes in  
291 emissivity and radiative forcing using a hierarchy of conceptual models. We show that the  
292 differing response of the lapse rate at high and low latitudes results in polar amplification.  
293 For fixed lapse rate, surface warming instead depends to first order only on the prescribed  
294 lapse rate (and not on the surface temperature). The differential Planck feedback alone  
295 therefore does not cause polar amplification, as it only compensates for a similarly weaker  
296 radiative forcing in response to increased atmospheric emissivity.

297 Radiative-advective equilibrium solutions provide a base-state model for the high-  
298 latitude thermal structure, and can be used to explore the atmospheric sensitivity to  
299 forcing. The high-latitude atmosphere is stable to convection, with an energy balance  
300 between cooling by longwave radiation and the sum of heating by direct solar absorption  
301 and atmospheric heat flux convergence. Radiative-advective equilibrium lapse rates are  
302 shown to increase strongly in response to surface heating or increasing atmospheric optical  
303 depth, leading to a positive lapse-rate feedback and amplified surface warming.

304 Radiative-convective equilibrium is used as a base-state model for the low-latitude ther-  
305 mal structure. The lapse rate is set by moist convection, and the response of the tem-  
306 perature profile to forcing does not depend on the vertical structure of the forcing; the  
307 new profile is simply a warmer or colder moist adiabat. The moist adiabatic lapse rate

308 decreases with warming, leading to a negative lapse-rate feedback and reduced surface  
309 warming.

310 Our results hold through a hierarchy of idealized column models in the absence of a  
311 water vapor feedback. When a water vapor feedback is included, the results for the lapse  
312 rate changes hold, but a strong low-latitude water vapor feedback leads to enhanced low-  
313 latitude warming, masking the polar amplification caused by meridional differences in  
314 the lapse-rate response. The lack of polar amplification in the presence of a water vapor  
315 feedback occurs only for the present climate and in the limit that clouds, the surface  
316 albedo feedback, and changes in atmospheric heat transport are neglected (any of which  
317 could restore polar amplification). In warmer climates, the high-latitude water vapor  
318 feedback might also have been strong [e.g. *Rose and Ferreira, 2013*]. The destabilization  
319 of high-latitude lapse rates in much warmer climates is also important for the onset of  
320 high-latitude deep convection [see also *Abbot and Tziperman, 2008*].

321 Our finding that high-latitude lapse rate changes depend on the nature of the forcing  
322 points to limitations of conventional top-of-atmosphere forcing-feedback analyses for un-  
323 derstanding high-latitude climate change. If we care about changes in surface temperature,  
324 then changes in the atmospheric lapse rate are a critical part of the solution. However,  
325 they depend not only on the top-of-atmosphere forcing, but also on the vertical struc-  
326 ture of that forcing. This finding may be relevant to understanding the role of clouds in  
327 high-latitude climate change, and their potential ability to alter surface temperature with  
328 little or no change in top-of-atmosphere energy balance. Consider, for instance, adding a  
329 cloud layer with a negative shortwave  $\delta F_S$  and a positive longwave  $\delta F_R$  that sum to zero;

330 the surface may still warm in response to this cloud layer (see Eqs. 17 and 19). We hope  
331 that future study of radiative-advective equilibrium, in more detailed models that include  
332 clouds and variability, will provide further insight into the high-latitude climate and how  
333 it responds to forcing.

334 **Acknowledgments.** We thank Tim Merlis and an anonymous reviewer for their help-  
335 ful comments on the manuscript. AEP was supported by a NSF Graduate Research  
336 Fellowship (grant DGE-1321846). MFJ was supported by a NOAA Climate and Global  
337 Change Postdoctoral Fellowship. TWC was supported by a NOAA Climate and Global  
338 Change Postdoctoral Fellowship and by the Harvard University Center for the Environ-  
339 ment. The presented work started as a summer project during the 2014 Geophysical Fluid  
340 Dynamics program at Woods Hole Oceanographic Institution. AEP and MFJ gratefully  
341 acknowledge support from the GFD program. Reanalysis used in this research is described  
342 in *Rienecker et al.* [2011]. Any additional data may be obtained from AEP.

## Notes

1. The water vapor feedback is estimated by subtracting the total feedback at fixed relative humidity,  $\lambda = \delta F_R^{LL} / \delta T_S =$   
4.3 W m<sup>-2</sup> / 2.4 K  $\approx$  1.8 W m<sup>-2</sup> K<sup>-1</sup>, from the temperature feedback, given by the sensitivity at fixed specific humidity:  
343  $\lambda_T = \delta F_R^{LL} / \delta T_S = 4.3$  W m<sup>-2</sup> / 0.8 K  $\approx$  5.4 W m<sup>-2</sup> K<sup>-1</sup>.

## References

- 344 Abbot, D. S., and E. Tziperman (2008), Sea ice, high-latitude convection, and equable  
345 climates, *Geophysical Research Letters*, *35*.
- 346 Abbot, D. S., and E. Tziperman (2009), Controls on the activation and strength of a  
347 high-latitude convective cloud feedback, *Journal of the Atmospheric Sciences*, *66*, 519

348 – 529.

349 Bintanja, R., Graverson, R. G., and W. Hazeleger (2011), Arctic winter warming am-  
350 plified by the thermal inversion and consequent low infrared cooling to space, *Nature*  
351 *Geoscience Letters*, *4*, 758 – 761.

352 Caballero, R., Mitchell, J., and M. Steder (2013), CliMT: An object-oriented climate  
353 modelling and diagnostics toolkit.

354 Chylek, P., Folland, C. K., Lesins, G., Dubey, M. K., and M.-Y. Wang (2009), Arctic air  
355 temperature change amplification and the Atlantic Multidecadal Oscillation, *Geophys-*  
356 *ical Research Letters*, *36*.

357 Graverson, R. G., Mauritsen, T., Tjernstrom, M., Kallen, E., and G. Svensson (2008),  
358 Vertical structure of recent Arctic warming, *Nature*, *451*, 53 – 56.

359 Graverson, R. G., and M. Wang (2009), Polar amplification in a coupled climate model  
360 with locked albedo, *Climate Dynamics*, *33*, 629 – 643.

361 Graverson, R. G., Langen, P. L., and T. Mauritsen (2014), Polar amplification in CCSM4:  
362 Contributions from the lapse rate and surface albedo feedbacks, *Journal of Climate*, *27*,  
363 4433 – 4450.

364 Hall, A. (2004), The role of surface albedo feedback in climate, *Journal of Climate*, *17*,  
365 1550 – 1568.

366 Hansen, J., Sato, M., and R. Ruedy (1997), Radiative forcing and climate response,  
367 *Journal of Geophysical Research*, *102*, 6831 – 6864.

368 Held, I. M. (1978), The tropospheric lapse rate and climatic sensitivity: Experiments with  
369 a two-level atmospheric model, *Journal of the Atmospheric Sciences*, *35*, 2083 – 2098.

- 370 Hwang, Y. T. and D. M. W. Frierson (2010), Increasing atmospheric poleward energy  
371 transport with global warming, *Geophysical Research Letters*, *37*.
- 372 Jansen, M. and R. Ferrari (2013), Equilibration of an atmosphere by adiabatic eddy fluxes,  
373 *Journal of the Atmospheric Sciences*, *70*, 2948 – 2962.
- 374 Lu, J., and M. Cai (2010), Quantifying contributions to polar warming amplification in  
375 an idealized coupled general circulation model, *Climate Dynamics*, *34*, 669 – 687.
- 376 Manabe, S., and R. T. Wetherald (1975), The effects of doubling the CO<sub>2</sub> concentration  
377 on the climate of a general circulation model, *Journal of the Atmospheric Sciences*, *32*.
- 378 Manabe, S., and R. J. Stouffer (1980), Sensitivity of a global climate model to an increase  
379 of CO<sub>2</sub> concentration in the atmosphere, *Journal of Geophysical Research*, *85*.
- 380 Meehl, G., et al. (2007), in *Climate Change 2007: The Physical Science Basis*, edited by  
381 S. Solomon et al., Cambridge University Press.
- 382 Miller, G. H., Alley, R. B., Brigham-Grette, J., Fitzpatrick, J. J., Polyak, L., Serreze,  
383 M. C., and J. W. White (2010), Arctic amplification: Can the past constrain the future?,  
384 *Quaternary Science Reviews*, *29*, 1779 – 1790.
- 385 Oort, A. H. (1974), Year-to-year variations in the energy balance of the Arctic, *Journal*  
386 *of Geophysical Research*, *79(9)*, 1253–1260.
- 387 Pithan, F., and T. Mauritsen (2014), Arctic amplification dominated by temperature  
388 feedbacks in contemporary climate models, *Nature Geoscience*, *7(3)*, 181-184
- 389 Serreze, M. C., Barrett, A. P., Slater, A. G., Steele, M., Zhang, J. and K. E. Trenberth  
390 (2007), The large-scale energy budget of the Arctic, *Journal of Geophysical Research*,  
391 *112*.

392 Soden, B. J., Held, I. M., Colman, R., Shell, K. M., Kiehl, J. T., and Shields, C. A. (2008),  
393 Quantifying climate feedbacks using radiative kernels, *Journal of Climate*, *21*(14), 3504-  
394 3520.

395 Rienecker, M. M., et al. (2011), MERRA - NASA's Modern-Era Retrospective Analysis  
396 for Research and Applications, *Journal of Climate*, *24*, 3624 – 3648.

397 Roe, G. H., Feldl, N., Armour, K. C., Hwang, Y. T., and Frierson, D. M. (2015), The  
398 remote impacts of climate feedbacks on regional climate predictability, *Nature Geo-*  
399 *science*, *8.2*, 135 – 139.

400 Rose, B. E., and D. Ferreira (2013), Ocean heat transport and water vapor greenhouse in  
401 a warm equable climate: A new look at the low gradient paradox, *Journal of Climate*,  
402 *26*, 2117 – 2136.

403 Screen, J. A., and I. Simmonds (2010), The central role of diminishing sea ice in recent  
404 Arctic temperature amplification, *Nature*, *464*, 1334 – 1337.

405 Trenberth, K. E., and J. M. Caron (2001), Estimates of meridional atmospheric and ocean  
406 heat transports, *Journal of Climate*, *14*, 3433–3443.

407 Winton, M. (2006), Amplified arctic climate change: What does surface albedo feedback  
408 have to do with it?, *Geophysical Research Letters*, *33*.

409 Vavrus, S. (2004), The impact of cloud feedbacks on Arctic climate under greenhouse  
410 forcing, *Journal of Climate*, *17*, 603 – 615.

411 Yang, X.-Y., Fyfe, J. C., and G. M. Flato (2010), The role of poleward energy transport  
412 in Arctic temperature evolution, *Geophysical Research Letters*, *37*.

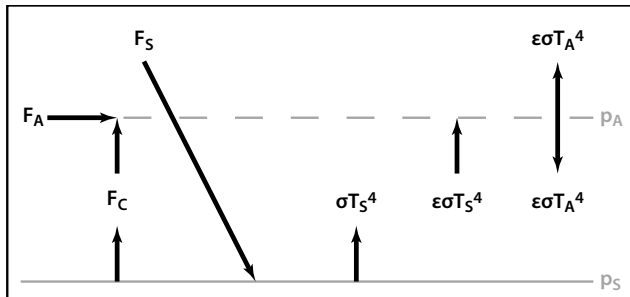


**Figure 1.** Illustration of a simple one-layer energy balance model with a surface ( $p_S = 1000$  hPa) and an atmospheric layer ( $p_A = 500$  hPa).  $F_S$  is the shortwave radiation absorbed by the surface,  $F_A$  is the sum of advective heat transport due to dynamics and atmospheric absorption of shortwave radiation,  $F_C$  is vertical convective heat transport,  $T_S$  is the temperature of the surface,  $T_A$  is the temperature of the atmospheric layer,  $\epsilon$  is the atmospheric emissivity and  $\sigma$  is the Stefan-Boltzmann constant.

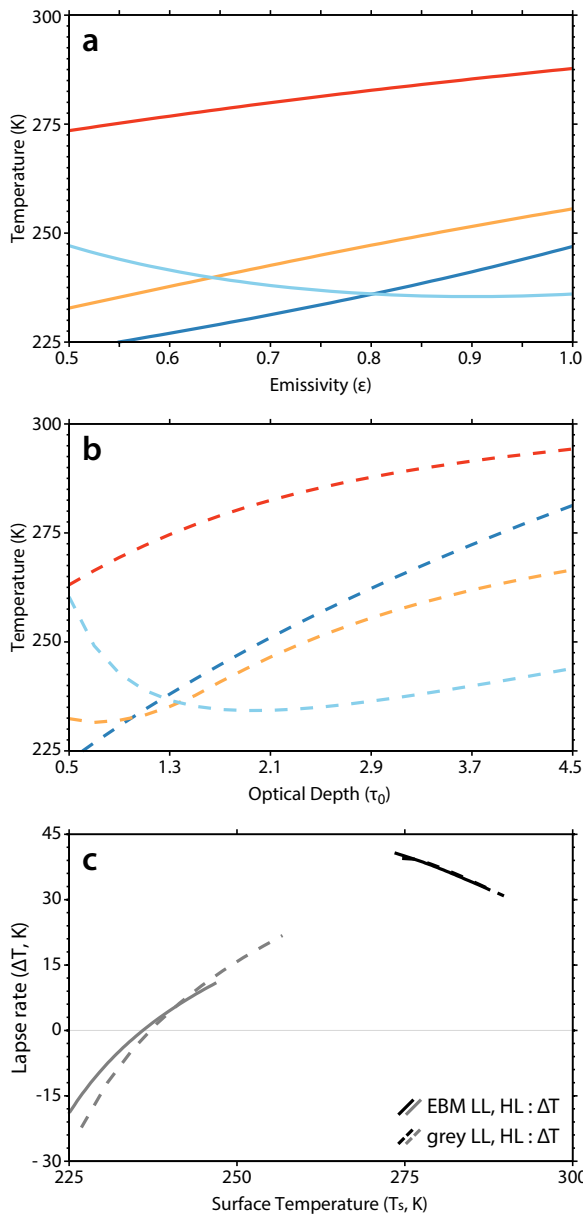


**Figure 2.** Comparison of the surface (LL, dark orange and HL, dark blue) and atmospheric (LL, light orange and HL, light blue) temperature response to increasing (a) emissivity in the EBM and (b) optical depth in the grey-gas model. A direct comparison of the lapse rates ( $\Delta_T = T_S - T_A$ ) for each model (EBM, solid lines and grey-gas model, dashed lines) for the high-latitude column (grey) and the low-latitude column (black) is shown in (c). In (c), we also limit the range of optical depths plotted to match the surface temperature range of the EBM; at low latitudes, we show  $\tau_0 = 1.3 - 3.3$ , and at high latitudes we show  $\tau_0 = 0.7 - 2.5$ .

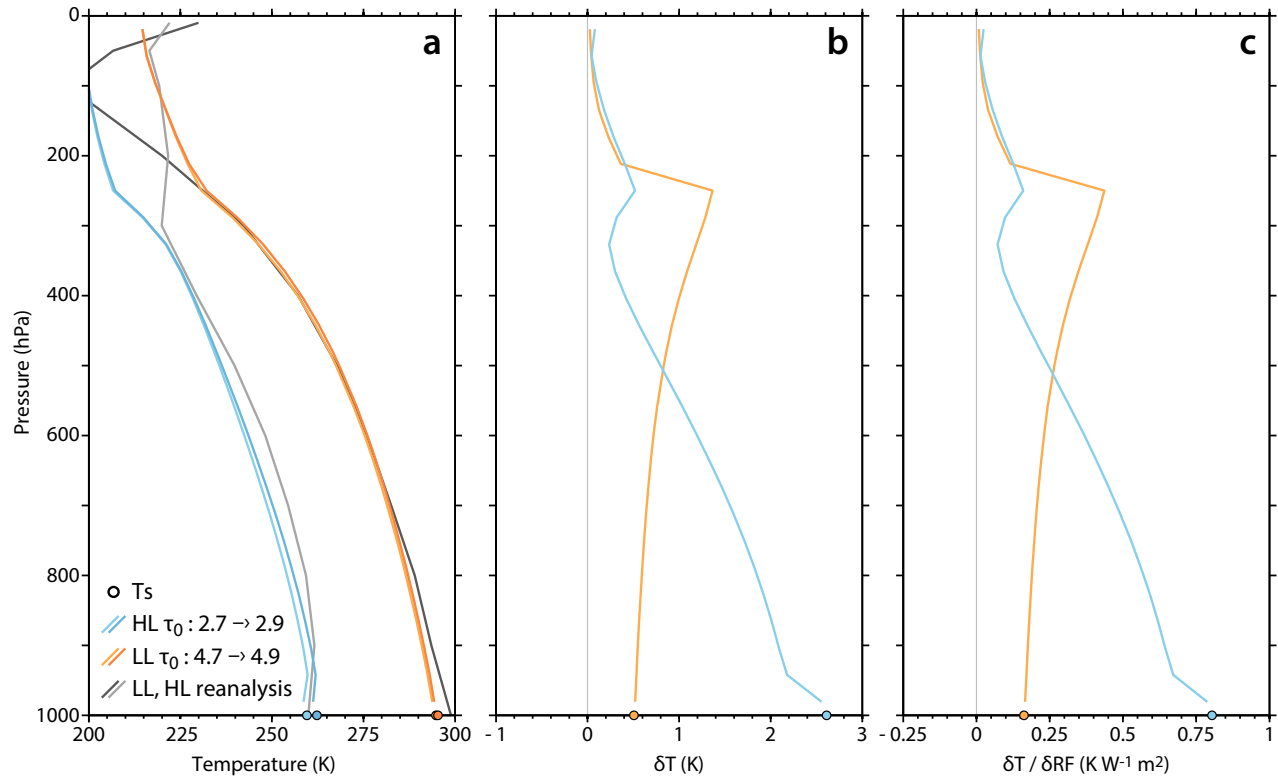


**Figure 3.** For the grey-gas model (a) high-latitude (blue,  $\tau_0$ : 2.7  $\rightarrow$  2.9) and low-latitude (orange,  $\tau_0$ : 4.7  $\rightarrow$  4.9) temperature profiles (solid lines) and surface temperatures (filled circles). Grey lines in (a) show reanalysis-derived temperature profiles for the current period (2010 - 2015). The temperature response for each region is shown in (b) and the temperature response normalized by radiative forcing is shown in (c).

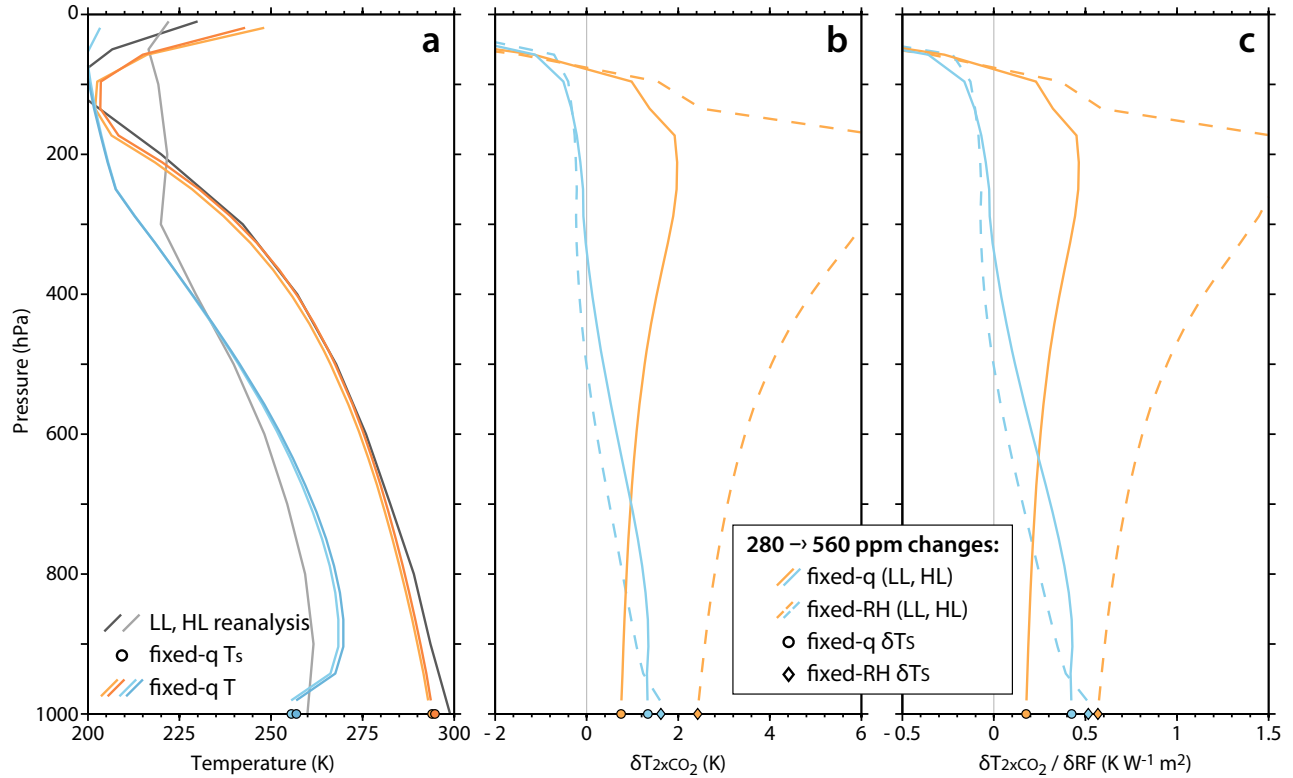


**Figure 4.** For the CCM3 radiative transfer model (a) high-latitude (blue,  $\text{CO}_2$ : 280 ppmv  $\rightarrow$  560 ppmv) and low-latitude (orange,  $\text{CO}_2$ : 280 ppmv  $\rightarrow$  560 ppmv) temperature profiles (solid lines) and surface temperatures (filled circles) at fixed specific humidity compared to reanalysis (grey) at 400 ppmv. Grey lines in (a) show reanalysis-derived temperature profiles for the current period (2010 - 2015). (b,c) As in Figs. 3b and 3c, but for  $\text{CO}_2$  doubling in two cases: (1) fixed specific humidity (fixed-q, dashed lines and filled circles) and (2) fixed relative humidity (fixed-RH, dashed lines and filled diamonds).